Nonlinear Interaction between the Drivers of the Monsoon and Summertime Stationary Waves

Chaim I. Garfinkel[1], Ian White[1], Edwin P. Gerber[2], Ori Adam[1], Martin Jucker[3]

Chaim I. Garfinkel, Fredy and Nadine Herrmann Institute of Earth Sciences, Hebrew University, Jerusalem, Israel (chaim.garfinkel@mail.huji.ac.il)

[1]Fredy and Nadine Herrmann Institute of Earth Sciences, Hebrew University, Jerusalem, Israel.

[2]Courant Institute of Mathematical Sciences, New York University, New York, USA

[3]Climate Change Research Center and ARC Centre of Excellence for Climate Extremes, University of New South Wales, Sydney, Australia

An intermediate complexity moist General Circulation Model is used to investigate the forcing of the Asian monsoon and the associated upper level anticyclone by land-sea contrast, net horizontal heat transport by the ocean, and topography. The monsoonal pattern is not simply the linear additive sum of the response to each forcing; only when all three forcings are included simultaneously does the monsoonal circulation extend westward to India. This nonadditivity impacts the location of the upper level anticyclone, which is shifted eastward and weaker if the forcings are imposed individually. Sahelian precipitation, and also austral summer precipitation over Australia, southern Africa, and South America, are likewise stronger if all forcings are imposed simultaneously. The source of the nonlinearity can be diagnosed using gross moist stability, but cannot be accounted for using the land-sea breeze paradigm. This non-additivity implies that the question of which forcing is most important is ill-posed.

1. Introduction

Monsoons dominate the climate in many regions of the tropics and subtropics, and are characterized by rainy summer and drier winter seasons. This rainfall is crucial for agriculture, among other societal implications, in heavily populated regions of the world. The monsoons are also a critical component of the large scale stationary wave pattern in summertime, and through the associated upper level anticyclone over Asia it regulates transport into the stratosphere [*Gill*, 1980; *Randel and Park*, 2006; *Vernier et al.*, 2015].

Traditionally, the localization of summertime rainfall near land led to the interpretation of monsoons as a large-scale sea-breeze, with moist air drawn over the warmer continent from the neighboring ocean, leading to convective rainfall over land [*Halley*, 1687], with a subsequent large-scale circulation driven by the convective heating [*Gill*, 1980]. This interpretation of monsoons as a sea breeze is seemingly contradicted by a few facts: land-sea temperature contrast peaks prior to monsoon onset over South Asia [*Simpson*, 1921], and interannual variability in land surface temperatures and total monsoonal precipitation are negatively correlated [*Kothawale and Kumar*, 2002]. More recent perspectives of monsoons view them as part of a "global monsoon mode" in which the tropical convergence zone migrates seasonally [*Trenberth et al.*, 2000; *Wang et al.*, 2009, 2017; *Geen et al.*, in press], with regional monsoons as localized and more extreme migrations due to a favorably-positioned continent [*Gadgil*, 2018] and due to orography, e.g., over Asia [*Li and Yanai*, 1996; *Chiang et al.*, 2020; *Acosta and Huber*, 2020]. In this view, a peak in near-surface moist static energy or equivalent potential temperature can accurately diagnose the seasonality and interannual variability in monsoonal precipitation [*Eltahir* *and Gong*, 1996; *Hurley and Boos*, 2013; *Ma et al.*, 2019] and more generally tropical convergence zones are located where the gross moist stability (i.e., the difference in moist static energy between the upper and lower troposphere) is small [*Neelin and Held*, 1987].

While both orography and land-sea contrast have been recognized as crucial for monsoons [see the discussion in *Xu et al.*, 2009], the relative importance of land-sea contrast and orography in forcing monsoons is less clear. *Xu et al.* [2009] find that zonal land-sea contrast and orography are of similar importance in determining the extent of Asian monsoon, though the meridional land-sea thermal contrast is relatively unimportant. However the model used by *Xu et al.* [2009] does not allow for examining the possible nonlinear interactions between these building blocks, and as shown in *Garfinkel et al.* [2020a], nonlinear interactions can be large in other seasons.

Several studies have aimed to delineate the fundamental dynamics of the monsoon using simplified models of the atmosphere, as this allows for isolating the relevant factors controlling the structure of tropical precipitation. Both dry axisymmetric models [e.g., *Bordoni and Schneider*, 2010; *Schneider and Bordoni*, 2008] and moist models with idealized continents [e.g., *Privé and Plumb*, 2007; *Bordoni and Schneider*, 2008; *Shaw*, 2014; *Maroon et al.*, 2016; *Geen et al.*, 2018, 2019; *Zhou and Xie*, 2018] have proven helpful in isolating the impact of specific forcings. The results from these studies bolster the view of monsoons as a local manifestation of the global tropical convergence zone. However, the relevance of the monsoon in these idealized models to Earth's monsoons remains unclear, as they generally cannot simulate the full meridional and zonal structure of observed monsoons.

Other studies have used more comprehensive models with full physics to identify the impact of orography in a given region [*Boos and Kuang*, 2010; *Chen and Bordoni*, 2014; *Wei and Bordoni*, 2016; *Baldwin et al.*, 2019], or to force surface temperature over continents to be similar to that of neighboring oceans [*Chao and Chen*, 2001], and then explore how monsoon strength and location changes. These comprehensive models, however, tend to be less flexible and are tuned such that removing too many relevant forcings leads to unstable behavior. A model that can fully bridge these two categories has, until very recently, been lacking, to the best of our knowledge.

While the aforementioned studies have made significant progress towards uncovering the building blocks of monsoons, there are still several open questions that we address in this study:

1. Can one reconstruct the full magnitude of monsoons by adding the individual building blocks, i.e. land-sea contrast, topography, and ocean heat fluxes, to a model with initially no zonally asymmetric bottom forcings?

2. To what extent do the various building blocks of monsoons interact nonlinearly with each other?

3. How does the degree of nonlinearity change regionally, for example between the South Asian (i.e. Indian subcontinent) and East Asian monsoons?

4. To the extent that nonlinearities exist, can we provide a diagnostic budget for the emergence of these nonlinearities using either the land-sea breeze paradigm or using moist static energy?

The goal of this work is to attempt to answer these four questions, and to then consider the implications for the summertime stationary waves. In order to achieve this goal, we use the simplified model developed in *Garfinkel et al.* [2020a] and *Garfinkel et al.* [2020b] that can represent the large scale structure of monsoonal precipitation. It is still modular enough, however, to allow one to build the monsoon by incrementally adding any or *all* relevant forcings (namely land-sea contrast, ocean heat fluxes, and orography) to a zonally symmetric aquaplanet, or to remove them incrementally from a model configuration in which all of the forcings are initially present.

After documenting the realism of the monsoons in the simplified model in Section 2, Section 3 demonstrates that for the South Asian monsoon, the individual building blocks interact non-additively, such that the sum of the responses to each building block does not equal the response when all are imposed simultaneously. Moist static energy and gross moist stability can provide an explanation for this non-additivity. Section 4 considers implications for the upper level anticyclone, and we summarize our findings in section 5.

2. The monsoon in a model of an idealized moist atmosphere (MiMA) version 2

We use the model of an idealized moist atmosphere (MiMA) introduced by *Jucker and Gerber* [2017], *Garfinkel et al.* [2020a], and *Garfinkel et al.* [2020b]. This model builds on the aquaplanet model of *Frierson et al.* [2006], *Frierson et al.* [2007], and *Merlis et al.* [2013]. Very briefly, the model solves the moist primitive equations on the sphere, employing a simplified Betts-Miller convection scheme [*Betts*, 1986; *Betts and Miller*, 1986], idealized boundary layer scheme based on Monin-Obukhov similarity theory, a purely thermodynamic, or slab, ocean, and the Rapid Radiative Transfer Model (RRTMG) radiation scheme [*Mlawer et al.*, 1997; *Iacono et al.*, 2000]. Please see *Jucker and Gerber* [2017] and *Garfinkel et al.* [2020b] for more details. The model is forced with CO_2 concentrations fixed at 390ppmv, and seasonally varying solar insolation.

Three sources of zonal asymmetry are added to the lower boundary of an initially zonally symmetric moist aquaplanet model: orography, prescribed ocean heat transport, and land-sea contrast (i.e., difference in heat capacity, surface friction, and moisture availability between oceans and continents). The specification of these forcings is identical to that in *Garfinkel et al.* [2020b], and is not repeated for brevity. This default model configuration is referred to as CONTROL for the rest of this paper (exp 7 on Table 1). Integrations with all possible combinations of these three forcings have been created, including an integration with none of the three forcings (hereafter no-forcing), and these integrations are summarized in Table 1. Note that all integrations (including the no-forcing integration) still include north-south ocean heat fluxes, as described in detail in *Garfinkel et al.* [2020b]. Unless otherwise indicated, all simulations in this paper were run with a triangular truncation at wavenumber 42 (T42; equivalent to a roughly 2.8° grid) with 40 vertical levels for 38 years after discarding at least 10 years as spinup.

The resulting climatological precipitation in June through September (JJAS) in CONTROL is shown in Figure 1bc, and observed precipitation sourced from the Global Precipitation Climatology Project (GPCP) version 2.3 is shown in Figure 1a. (The precipitation in each experiment in Table 1 is shown in supplemental Figure 1). The climatological stationary waves in CONTROL and in the ERA-5 reanalysis [*Hersbach et al.*, 2020] quantified using 200hPa geopotential height and streamfunction are shown in supplemental figures 2 and 3. Precipitation over South and East Asia is of similar magnitude to that observed (Figure 1a), and largely occurs in the correct location, though Gibbs phenomena associated with the Tibetan Plateau are evident at T42 (and even T85) resolution as east-west oriented bands of enhanced and reduced precipitation. CONTROL captures the upper level anticyclone above the monsoon in essentially the correct location and with a reasonable magnitude, though there is a bias over Mongolia and Southeastern Russia (likely associated with anomalously strong precipitation in this region). While some of the fine scale structure of precipitation and the stationary waves is not captured, our focus in this paper will be on larger scale differences (e.g., between South and East Asia). While not perfect, we consider our model a useful tool to understand how orography, ocean horizontal heat fluxes, and land-sea contrast interact to form the monsoon.

3. Non-additivity of the monsoon

We first consider whether the monsoon can be decomposed linearly into the response to the various forcings. Figure 2a shows the difference in precipitation between CONTROL and an experiment with no zonally asymmetric forcings (exp 0 on Table 1). For Figure 2b, we first calculate the responses when each of the forcings is added separately to no-forcing, that is, the difference between topography only and no-forcing, ocean heat fluxes only and no-forcing, and land-sea contrast only and no-forcing. We then sum the precipitation response in these three individual forcing experiments. The net effect is that Figure 2b shows the precipitation response to the three forcings when the response to each forcing is computed in isolation. While the precipitation over East Asia in CONTROL appears to be associated with the linear summation of the forcings, the precipitation over India and the Sahel is much stronger when the forcings interact.

Which forcings are most responsible for the non-additive behavior? Before proceeding we review the definition of the isolated and full nonlinear response of *Held et al.* [2002]. The response to some source of asymmetry A in MiMA can be denoted as $M(A)$. Let F represent all three forcings in the most realistic configuration such that the response to F is $M(F)$. As in *Held et al.* [2002], we refer to $M(A)$ as the isolated nonlinear response to A and $M(F)$ - $M(F$ - $A)$ as the full nonlinear response to A. That is, the isolated nonlinear response to A occurs when A is added first to a configuration with none of the three forcings, while the full nonlinear response to A occurs when A is added to a configuration that already has the other two forcings (or is the first to be removed from CONTROL).

The bottom three rows of Figure 2 show the precipitation response to each forcing imposed in isolation (right column; *isolated nonlinear response*) and also when each forcing is removed from CONTROL (left column; the *full nonlinear response*). For example, Figure 2c considers the difference in precipitation between CONTROL and the experiment where both land-sea contrast and topography are imposed but ocean heat flux zonal asymmetry is not. Hence, the precipitation response in Figure 2c is that forced by ocean heat flux zonal asymmetries when imposed on a basic state that already includes land-sea contrast and topography (the *full nonlinear response*). This pattern in Figure 2c can be compared to the *isolated nonlinear* response to ocean heat flux zonal asymmetries in Figure 2d. Ocean heat flux zonal asymmetries in isolation have a limited impact on the precipitation in monsoonal regions, but if imposed on the basic state set up by topography and land-sea contrast, ocean heat flux zonal asymmetries lead to a strengthened monsoon over South and East Asia and enhanced precipitation over the Sahel.

Figure 2e shows the impact that topography has on precipitation when imposed on a basic-state that already includes land-sea contrast and east-west ocean heat fluxes, while Figure 2f shows the isolated nonlinear response to topography. Precipitation is limited to East Asia in the isolated nonlinear response, but extends over India in the full nonlinear response. Figure 2g shows the full nonlinear response to land-sea contrast, while Figure 2h shows the isolated nonlinear response. The isolated nonlinear response is weaker than the full nonlinear response in all monsoonal regions, with the differences particularly pronounced over South Asia: there is no Indian monsoon in the isolated nonlinear response. Similar non-additivity is evident if we consider omega at 500hPa (supplemental Figure S4) instead of precipitation: the response to each forcing, and especially to land-sea contrast, depends on the background state on which it is imposed.

Due to the strong non-additivity, one must be cautious in ranking the relative importance of the factors as the forcings interact. However there is a general indication that topography and land-sea contrast are more important over South and East Asia than east-west oceanic heat transport, while all three are important over the Sahel. The overall importance of each factor can be succinctly summarized in the Taylor diagram [*Taylor*, 2001] in Figure 3a. The reference state for the Taylor diagram is the difference between CONTROL and no forcing in figure 2a, to which we then compare the isolated and full nonlinear responses to each forcing and also the sum of the isolated nonlinear and the sum of the full nonlinear responses. The full nonlinear responses to each forcing are closer to the total response than the accompanying isolated nonlinear responses, and topography (TOP) and land-sea contrast (LSC) are more important that oceanic heat transport (OHT).

In order to understand these nonlinearities, we consider the gross moist stability [GMS; *Neelin and Held*, 1987; *Raymond et al.*, 2009] of the atmosphere. The uses of GMS are discussed in detail in *Neelin and Held* [1987] and *Raymond et al.* [2009], but briefly, convection is expected to be located in regions with small (but positive) GMS, with dry conditions expected in regions with relatively high GMS. Furthermore, the strength of the convective response to a given external perturbation at the surface is inversely proportional to the GMS; that is, an energy flux into the atmosphere will have a stronger response if located in a region with smaller GMS.

In the form of *Neelin and Held* [1987], GMS is defined as the difference between the vertically integrated moist static energy above the mid-troposphere and the vertically integrated moist static energy below the mid-troposphere, with the weight assigned to each level proportional to the divergence at that level [equation 2.6 of *Neelin and Held*, 1987]. Here we use a much simplified version of this metric: the difference in moist static energy at 250hPa versus 850hPa, the two levels chosen to represent the upper and lower troposphere. The results are similar though noisier if we use the original definition, and are also similar if we choose levels adjacent to 250hPa and 850hPa. GMS in CONTROL is generally low in regions with strong monsoonal precipitation (Figure 4a) as expected.

Why are there nonlinearities in the response of the monsoon to these forcings? We first focus on why the response to oceanic heat transport is stronger if imposed on a basic state that includes the other forcings (Figure 2cd). The GMS for the integration with no bottom forcings is shown in Figure 4b, while the GMS for the integration with land-sea contrast and topography included is shown in Figure 4c. GMS is clearly lower over South and East Asia in Figure 4c than in Figure 4b, and thus can explain the non-additive response. That is, the reduced GMS over Asia makes the atmosphere more sensitive to perturbations, amplifying the impact of oceanic heat transport on the monsoons. Therefore, the response is larger in Figure 2c than in Figure 2d. The GMS is also lower over the Sahel and East Africa in Figure 4c than in Figure 4b, and thus can account for the non-additive behavior in precipitation in this region too.

GMS can also explain the stronger response to topography if imposed on a background state that already includes ocean heat flux zonal asymmetries and land-sea contrast. The GMS for the integration with ocean heat flux zonal asymmetries and land-sea contrast is shown in Figure 4e. GMS is lower over South and East Asia and Africa in Figure 4e than in Figure 4b, and thus the response to topography is stronger in Figure 2e than in Figure 2f. Finally, the GMS is lower over South and East Asia in the integration with ocean heat flux zonal asymmetries and topography than in the integration with no zonally asymmetric bottom forcings (Figure 4g vs Figure 4b), explaining the stronger response to the land-sea contrast in Figure 2g than in Figure 2h. While the focus of this paper is on boreal summer monsoons, December-February precipitation over South America, southern Africa, and Australia is stronger if the forcings are imposed on a basic state that already includes the other forcings (figure 2b), and this effect is consistent with GMS (not shown).

Of the three forcings, ocean heat flux zonal asymmetries are least important for changes in GMS over South and East Asia. This can be inferred by comparing GMS in CONTROL (Figure 4a) with GMS in the integration with topography and land-sea contrast (Figure 4c), and also by noting that of the three individual forcing simulations in Figure 4dfh, the ocean heat flux zonal asymmetries integration (Figure 4d) is most similar to the no-forcing integration (Figure 4b). Over Africa, topography is most important for East Africa, while ocean heat flux zonal asymmetries are more important further west.

Overall, the individual building blocks of monsoons interact non-additively, such that the sum of the responses to each building block does not equal the response when all are imposed simultaneously. Gross moist stability can provide an explanation for this non-additivity. Nonlinear effects are particularly pronounced over South Asia and weaker over East Asia.

4. Impact on NH summer stationary waves

The non-additivity observed in section 3 for precipitation has implications for the upper-level anticyclone. It is well established that the upper-level anticyclone is driven by convection [*Gill*, 1980; *Randel and Park*, 2006], and hence it is reasonable to suspect a non-additive response to the building blocks of the antiyclcone similar to that seen for precipitation. This expectation is confirmed in Figure 5, which mirrors Figure 2 but for 200hPa streamfunction. Figure 5a and 5b compare stationary waves in CONTROL to the sum of the stationary wave pattern in the topography only, ocean heat fluxes only, and land-sea contrast only experiments. Consistent with the weakness of the precipitation over India and the Sahel in Figure 2b, the ridge over the Tibetan Plateau is not present in Figure 5b and a trough is evident over the Northern Sahara. Similar figures for streamfunction at 850hPa and height at 200hPa are included in supplemental Figure S5 and S6, and they too show a non-additive response.

The bottom three rows of Figure 5 show response to each forcing imposed in isolation (right column; *isolated nonlinear response*) and also when each forcing is removed from CONTROL (left column; the *full nonlinear response*). Zonal asymmetries in oceanic heat transport impact only the eastward extension of the ridge towards the South China Sea, and have a relatively small impact on the upper-level anticyclone over the Tibetan Plateau in both the isolated and full nonlinear response, consistent with their comparatively smaller impact on precipitation. The impact over the South China Sea is stronger in the isolated nonlinear response, consistent with the localization of the precipitation response in this region. Figure 5e shows the influence of topography on stationary waves when imposed on a basic-state that already includes land-sea contrast and east-west ocean heat fluxes, while Figure 5f shows the isolated nonlinear response to topography. The impact of topography is limited to South Asia in the isolated nonlinear response, but extends to the west in the full nonlinear response where it contributes to the westward extension of the Asian anti-cyclone. Figure 5g shows the full nonlinear response to land-sea contrast, while Figure 5h shows the isolated nonlinear response. Consistent with the lack of a monsoon over South Asia in the isolated nonlinear response, the ridge is confined to East Asia in Figure 5h and does not extend to Western Asia. Similar results are evident for streamfunction at 850hPa and height at 200hPa (supplemental Figure S5 and S6).

It is worth noting that the sum of the full nonlinear responses does not equal the stationary waves in CONTROL (not shown), just as the sum of the isolated nonlinear responses does not equal the stationary waves in CONTROL (Figure 5b). Such a lack of additivity is evident for precipitation as well (Figure 3a). Hence it thus not meaningful to rank the importance of the various building blocks, though both the isolated nonlinear and full nonlinear responses to land-sea contrast exceed that in response to topography and ocean heat flux zonal asymmetries at 200hPa, while at 850hPa topography and land-sea contrast play a similar role (supplemental Figure S6).

5. Discussion and Conclusions

Monsoon rainfall is crucial for food security in heavily populated regions of the world. While comprehensive models with realistic land-sea contrast and orography simulate these monsoons, it can be difficult to delineate which specific building block in these models is most important for the monsoons. To our knowledge, little work has been done on the possibility of non-additive behavior among these building blocks. Simpler models (e.g., moist models with idealized continents) have been used to assess how these individual building blocks lead to monsoons, but these models typically cannot simulate the meridional and zonal structure of observed monsoons. Here, we bridge this gap with a model that can represent the large scale structure of monsoonal precipitation with fidelity, yet allows us one to build this monsoonal structure by incrementally adding any or *all* relevant building blocks (namely land-sea contrast, ocean heat fluxes, and orography) to a zonally symmetric aquaplanet. As shown in the text, it is equally instructive to incrementally remove the individual building blocks from a model configuration in which all are initially present.

We now summarize the answers to the questions asked in the introduction. The various building blocks of the monsoons interact nonlinearly with each other. Specifically, the response to all three building blocks is considerably weaker if they are added individually to a zonally symmetric aquaplanet, as compared to a configuration in which the other building blocks are already present. This effect is particularly pronounced over South Asia, and less so over East Asia. The question of which forcing is most important is ill-posed in regions with pronounced non-additivity, but generally east-west ocean heat fluxes are less important over Asia, while topography is less important over West Africa.

This non-additivity can be interpreted in all regions using moist static energy and gross moist stability. In contrast, the land-sea breeze model cannot explain the monsoonal response to land-sea contrast or orography. We demonstrate this by considering the surface temperature response to the individual building blocks in supplemental Figure 7, and our specific focus is on the full nonlinear and isolated nonlinear responses to land-sea contrast (Figure S7e vs S7f). The surface temperature response to land-sea contrast is actually larger if land-sea contrast is imposed on a basic state lacking any of the forcings than when imposed on a basic state that already has the other two forcings (Figure S7e vs S7f). Hence, the land-sea breeze model would suggest a stronger monsoon for the isolated nonlinear response to land-sea contrast, the opposite of what actually occurs. Hence, only an energetic perspective is helpful for understanding the non-additivity of the responses.

While the model employed here can represent the large scale structure of summer precipitation, it has its limitations. In addition to the simplification to physical processes detailed in Section 2 and *Garfinkel et al.* [2020b] (e.g., soil moisture, clouds, convection), the east-west transport of heat by the ocean is not coupled to the surface winds, which may lead to an underestimation of their importance [*Lutsko et al.*, 2019]. Nevertheless, our key result - there is significant nonlinear interaction among the building blocks - highlights the challenge the monsoonal circulation poses to couple climate modeling: biases in one component of the response will impact all other forcings, making it challenging to diagnose the source of the error. Atmosphere-only model integrations of the "total nonlinear" response, however, can help by providing the fingerprint of biases in each component of the system.

Acknowledgments. CIG, IW, and ME acknowledge the support of a European Research Council starting grant under the European Union Horizon 2020 research and innovation programme (grant agreement number 677756). EPG acknowledges support from the US NSF through grant AGS 1852727. MJ acknowledges support from the Australian Research Council (ARC) Centre of Excellence for Climate Extremes (CE170100023) and ARC grant FL 150100035. Correspondence and requests for data should be addressed to C.I.G. (email: chaim.garfinkel@mail.huji.ac.il).

References

Acosta, R., and M. Huber (2020), Competing topographic mechanisms for the summer indo-asian monsoon, *Geophysical Research Letters*, *47*(3), e2019GL085,112.

Baldwin, J. W., G. A. Vecchi, and S. Bordoni (2019), The direct and ocean-mediated influence of asian orography on tropical precipitation and cyclones, *Climate dynamics*, *53*(1-2), 805–824.

Betts, A., and M. Miller (1986), A new convective adjustment scheme. part ii: Single column tests using gate wave, bomex, atex and arctic air-mass data sets, *Quarterly Journal of the Royal Meteorological Society*, *112*(473), 693–709, doi:10.1002/qj.49711247308.

Betts, A. K. (1986), A new convective adjustment scheme. part i: Observational and theoretical basis, *Quarterly Journal of the Royal Meteorological Society*, *112*(473), 677–691, doi:10.1002/qj.49711247307.

Boos, W. R., and Z. Kuang (2010), Dominant control of the south asian monsoon by orographic insulation versus plateau heating, *Nature*, *463*(7278), 218–222.

Bordoni, S., and T. Schneider (2008), Monsoons as eddy-mediated regime transitions of the tropical overturning circulation, *Nature Geoscience*, *1*(8), 515–519.

Bordoni, S., and T. Schneider (2010), Regime transitions of steady and time-dependent hadley circulations: Comparison of axisymmetric and eddy-permitting simulations, *Journal of the Atmospheric Sciences*, *67*(5), 1643–1654.

Chao, W. C., and B. Chen (2001), The Origin of Monsoons, *Journal of the Atmospheric Sciences*, *58*(22), 3497–3507, doi:10.1175/1520-0469(2001)058⟨3497:TOOM⟩2.0.CO;2.

Chen, J., and S. Bordoni (2014), Orographic effects of the tibetan plateau on the east asian summer monsoon: An energetic perspective, *Journal of Climate*, *27*(8), 3052–3072.

Chiang, J., W. Kong, C. Wu, and D. Battisti (2020), Origins of east asian summer monsoon seasonality, *Journal of Climate*, *33*(18), 7945–7965.

Eltahir, E. A., and C. Gong (1996), Dynamics of wet and dry years in west africa, *Journal of climate*, *9*(5), 1030–1042.

Frierson, D. M., I. M. Held, and P. Zurita-Gotor (2006), A gray-radiation aquaplanet moist gcm. part i: Static stability and eddy scale, *Journal of the atmospheric sciences*, *63*(10), 2548–2566, doi:10.1175/JAS3753.1.

Frierson, D. M., I. M. Held, and P. Zurita-Gotor (2007), A gray-radiation aquaplanet moist gcm. part ii: Energy transports in altered climates, *Journal of the atmospheric sciences*, *64*(5), 1680–1693, doi:10.1175/JAS3913.1.

Gadgil, S. (2018), The monsoon system: Land–sea breeze or the itcz?, *Journal of Earth System Science*, *127*(1), 1, doi:https://doi.org/10.1007/s12040-017-0916-x.

Garfinkel, C. I., I. P. White, E. P. Gerber, and M. Jucker (2020a), The building blocks of northern hemisphere wintertime stationary waves, *Journal of Climate*, *33*(13), doi:10.1175/JCLI-D-19-0181.1.

Garfinkel, C. I., I. White, E. P. Gerber, and M. Jucker (2020b), The impact of sst biases in the tropical east pacific and agulhas current region on atmospheric stationary waves in the southern hemisphere, *Journal of Climate*, *33*(21), 9351–9374.

Geen, R., F. Lambert, and G. Vallis (2018), Regime change behavior during asian monsoon onset, *Journal of Climate*, *31*(8), 3327–3348.

Geen, R., F. H. Lambert, and G. K. Vallis (2019), Processes and timescales in onset and withdrawal of "aquaplanet monsoons", *Journal of the Atmospheric Sciences*, *76*(8), 2357–2373.

Geen, R., S. Bordoni, D. S. Battisti, and K. Hui (in press), Monsoons, itczs and the concept of the global monsoon, *Reviews of Geophysics*, p. e2020RG000700.

Gill, A. E. (1980), Some simple solutions for heat-induced tropical circulation, *Quarterly Journal of the Royal Meteorological Society*, *106*, 447–462, doi:10.1002/qj.49710644905.

Halley, E. (1687), An historical account of the trade winds, and monsoons, observable in the seas between and near the tropicks, with an attempt to assign the physical cause of the said winds, *Philosophical Transactions of the Royal Society of London*, *16*(183), 153–168, doi:https://doi.org/10.1098/rstl.1686.0026.

Held, I. M., M. Ting, and H. Wang (2002), Northern winter stationary waves: Theory and modeling, *Journal of climate*, *15*(16), 2125–2144.

Hersbach, H., et al. (2020), The era5 global reanalysis, *Quarterly Journal of the Royal Meteorological Society*, *146*(730), 1999–2049.

Hurley, J. V., and W. R. Boos (2013), Interannual variability of monsoon precipitation and local subcloud equivalent potential temperature, *Journal of climate*, *26*(23), 9507–9527.

Iacono, M. J., E. J. Mlawer, S. A. Clough, and J.-J. Morcrette (2000), Impact of an improved longwave radiation model, rrtm, on the energy budget and thermodynamic properties of the ncar community climate model, ccm3, *Journal of Geophysical Research: Atmospheres*, *105*(D11), 14,873–14,890.

Jucker, M., and E. Gerber (2017), Untangling the annual cycle of the tropical tropopause layer with an idealized moist model, *Journal of Climate*, *30*(18), 7339–7358.

Kothawale, D., and K. R. Kumar (2002), Tropospheric temperature variation over india and links with the indian summer monsoon: 1971-2000, *Mausam*, *53*(3), 289–308.

Li, C., and M. Yanai (1996), The onset and interannual variability of the asian summer monsoon in relation to land–sea thermal contrast, *Journal of Climate*, *9*(2), 358–375.

Lutsko, N. J., J. Marshall, and B. Green (2019), Modulation of monsoon circulations by cross-equatorial ocean heat transport, *Journal of Climate*, *32*(12), 3471–3485.

Ma, D., A. H. Sobel, Z. Kuang, M. S. Singh, and J. Nie (2019), A moist entropy budget view of the south asian summer monsoon onset, *Geophysical Research Letters*, *46*(8), 4476–4484.

Maroon, E. A., D. M. W. Frierson, S. M. Kang, and J. Scheff (2016), The Precipitation Response to an Idealized Subtropical Continent, *Journal of Climate*, *29*(12), 4543–4564, doi:10.1175/JCLI-D-15-0616.1.

Merlis, T. M., T. Schneider, S. Bordoni, and I. Eisenman (2013), Hadley circulation response to orbital precession. part ii: Subtropical continent, *Journal of Climate*, *26*(3), 754–771.

Mlawer, E. J., S. J. Taubman, P. D. Brown, M. J. Iacono, and S. A. Clough (1997), Radiative transfer for inhomogeneous atmospheres: Rrtm, a validated correlated-k model for the longwave, *Journal of Geophysical Research: Atmospheres*, *102*(D14), 16,663–16,682.

Neelin, J. D., and I. M. Held (1987), Modeling Tropical Convergence Based on the Moist Static Energy Budget, *Monthly Weather Review*, *115*(1), 3–12, doi:10.1175/1520-0493(1987)115⟨0003:MTCBOT⟩2.0.CO;2.

Privé, N. C., and R. A. Plumb (2007), Monsoon dynamics with interactive forcing. part i: Axisymmetric studies, *Journal of the atmospheric sciences*, *64*(5), 1417–1430.

Randel, W. J., and M. Park (2006), Deep convective influence on the asian summer monsoon anticyclone and associated tracer variability observed with atmospheric infrared sounder (airs), *Journal of Geophysical Research: Atmospheres*, *111*(D12).

Raymond, D. J., S. L. Sessions, A. H. Sobel, and Ž. Fuchs (2009), The mechanics of gross moist stability, *Journal of Advances in Modeling Earth Systems*, *1*(3).

Schneider, T., and S. Bordoni (2008), Eddy-mediated regime transitions in the seasonal cycle of a hadley circulation and implications for monsoon dynamics, *Journal of the Atmospheric Sciences*, *65*(3), 915–934.

Shaw, T. A. (2014), On the role of planetary-scale waves in the abrupt seasonal transition of the northern hemisphere general circulation, *Journal of the Atmospheric Sciences*, *71*(5), 1724–1746.

Simpson, G. (1921), The south-west monsoon, *Quarterly Journal of the Royal Meteorological Society*, *47*(199), 151–171, doi:https://doi.org/10.1002/qj.49704719901.

Taylor, K. E. (2001), Summarizing multiple aspects of model performance in a single diagram, *Journal of Geophysical Research: Atmospheres*, *106*(D7), 7183–7192.

Trenberth, K. E., D. P. Stepaniak, and J. M. Caron (2000), The global monsoon as seen through the divergent atmospheric circulation, *Journal of Climate*, *13*(22), 3969–3993, doi:https://doi.org/10.1175/1520-0442(2000)013⟨3969:TGMAST⟩2.0.CO;2.

Vernier, J.-P., T. Fairlie, M. Natarajan, F. Wienhold, J. Bian, B. Martinsson, S. Crumeyrolle, L. Thomason, and K. Bedka (2015), Increase in upper tropospheric and lower stratospheric aerosol levels and its potential connection with asian pollution, *Journal of Geophysical Research: Atmospheres*, *120*(4), 1608–1619.

Wang, B., Q. Ding, and P. Joseph (2009), Objective definition of the indian summer monsoon onset, *Journal of Climate*, *22*(12), 3303–3316, doi:https://doi.org/10.1175/2008JCLI2675.1.

Wang, P. X., B. Wang, H. Cheng, J. Fasullo, Z. Guo, T. Kiefer, and Z. Liu (2017), The global monsoon across time scales: Mechanisms and outstanding issues, *Earth-Science Reviews*, *174*, 84–121.

Wei, H.-H., and S. Bordoni (2016), On the role of the african topography in the south asian monsoon, *Journal of the Atmospheric Sciences*, *73*(8), 3197–3212.

Xu, Z., C. Fu, and Y. Qian (2009), Relative Roles of Land–Sea Distribution and Orography in Asian Monsoon Intensity, *Journal of the Atmospheric Sciences*, *66*(9), 2714–2729, doi:10.1175/2009JAS3053.1.

Zhou, W., and S.-P. Xie (2018), A hierarchy of idealized monsoons in an intermediate gcm, *Journal of Climate*, *31*(22), 9021–9036.

Table 1. MiMA Experiments, with “Y” indicating a forcing is on and “N” indicating a forcing is off. The isolated nonlinear response to topography can be deduced from experiment 1, while the full nonlinear response is the difference between experiments 7 and 6. The isolated nonlinear response to land-sea contrast can be deduced from experiment 2, while the full nonlinear response is the difference between experiments 7 and 4. The isolated nonlinear response to ocean heat fluxes can be deduced from experiment 3, while the full nonlinear response is the difference between experiments 7 and 5.

Table: MiMA Model experiments

	orography	land-sea contrast	ocean heat fluxes
exp 0	N	N	N
exp 1	Y	N	N
exp 2	N	Y	N
exp 3	N	N	Y
exp 4	Y	N	Y
exp 5	Y	Y	N
exp 6	N	Y	Y
exp 7 (CONTROL)	Y	Y	Y

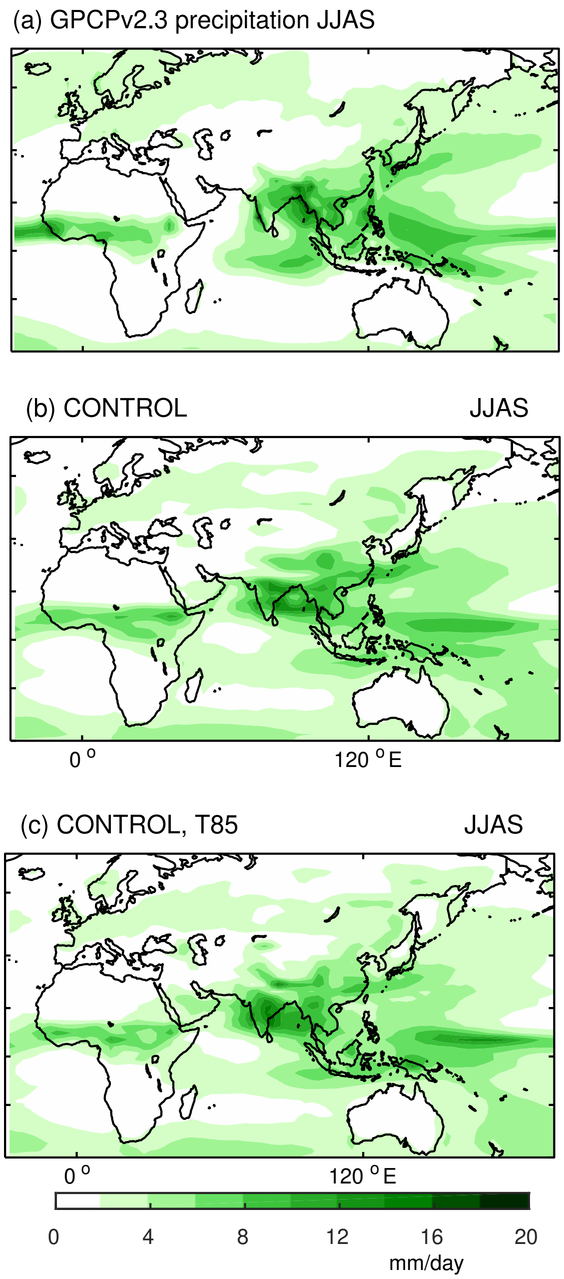

Figure 1. Precipation in JJAS (a) in GPCPv2.3, (b) in the CONTROL integration with T42 resolution, and in (c) the CONTROL integration with double the horizontal resolution (T85). The contour interval is 2mm/day.

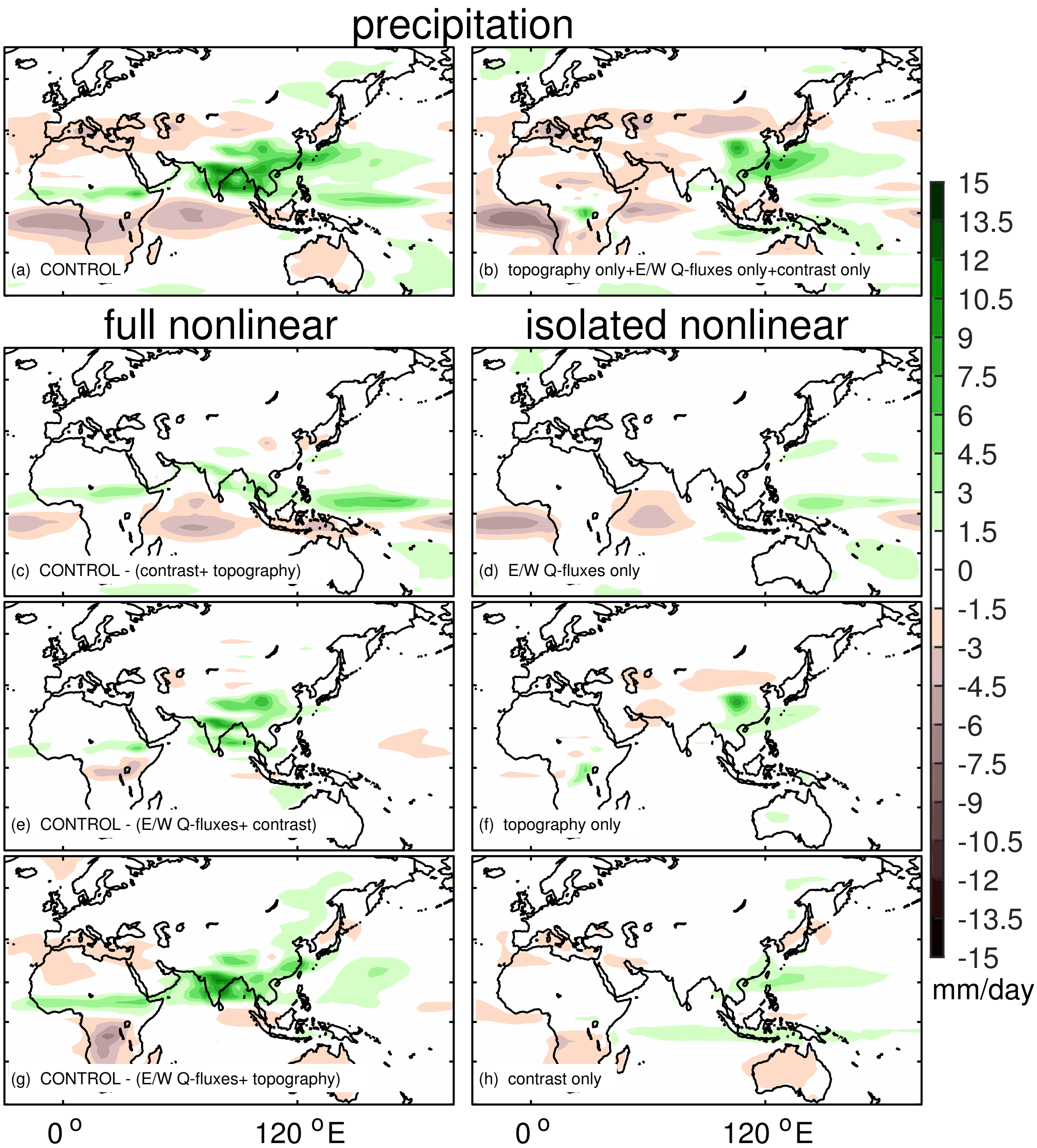

Figure 2. Precipitation in June-September (a) in CONTROL as compared to no-forcing, (b) as in (a) but for the sum of integrations with topography only, land-sea contrast only, and ocean heat fluxes only as compared to no-forcing; (c) the difference between CONTROL and the integration with land-sea contrast and topography; (d) integration with only ocean heat fluxes as compared to no-forcing; (e) the difference between CONTROL and the integration with ocean heat fluxes and land-sea contrast; (f) integration with only topography as compared to no-forcing; (g) the difference between CONTROL and the integration with ocean heat fluxes and topography; (h) integration with only land-sea contrast as compared to no-forcing. The contour interval is 1.5mm/day.

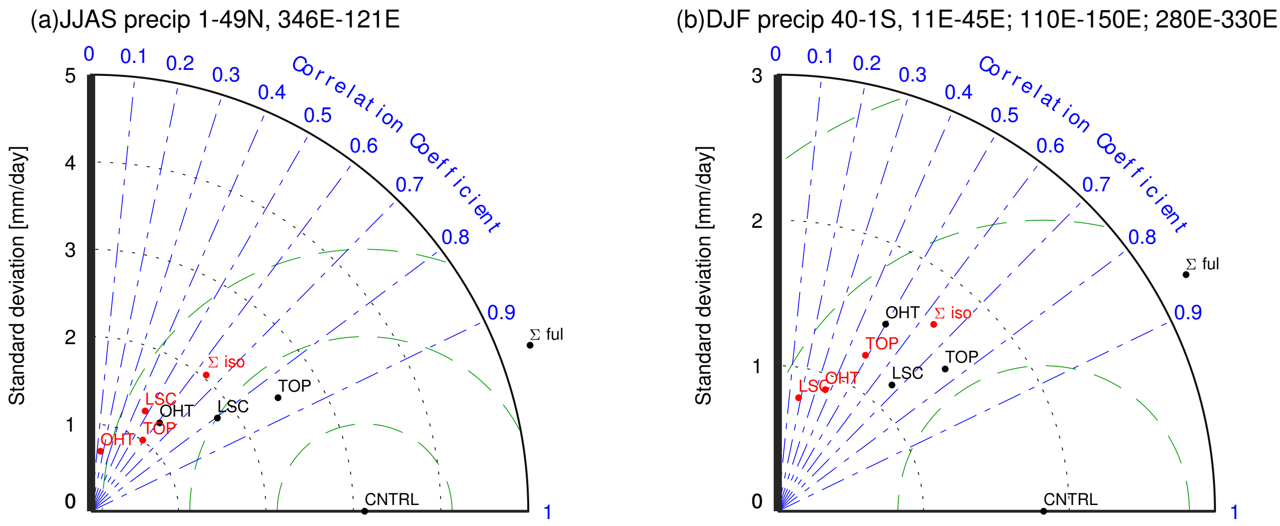

Figure 3. Taylor diagram of the precipitation response to each forcing, using the difference between CONTROL and no-forcing as the reference. The (red) isolated and (black) full nonlinear response to topography (TOP), land-sea contrast (LSC), and oceanic heat transport (OHT), as well as the sum of the isolated nonlinear (Σiso) and sum of the full nonlinear responses (Σful), are shown. (a) Northern Hemisphere from 1N to 49N and 346E to 121E; (b) in December through February from 1S to 40S and 11E to 45E (Africa), 110E-150E (Australia), and 280E-330E (South America). Isolines of the centered root mean square difference equal to 1, 2, and 3mm/day are shown in green.

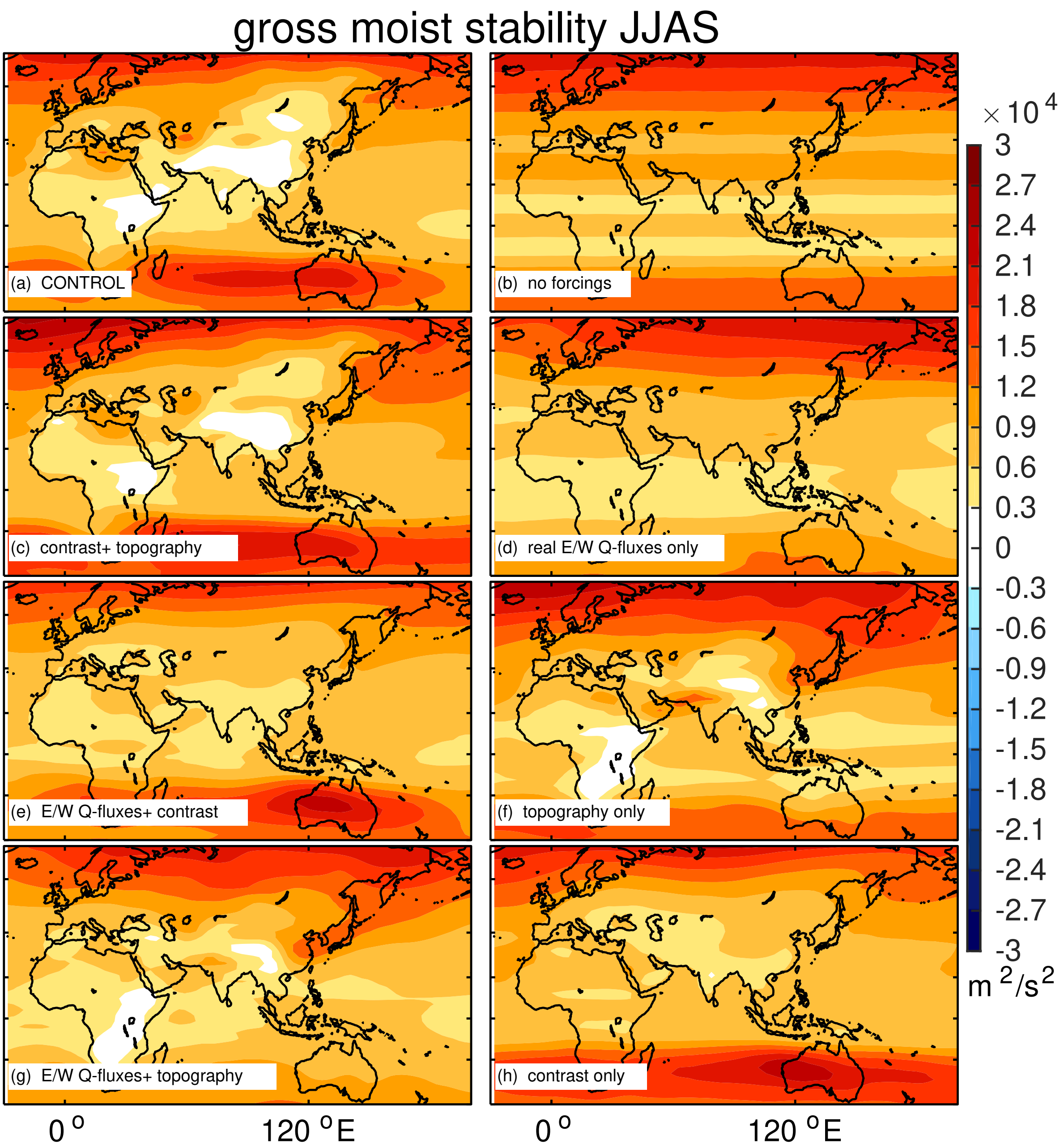

Figure 4. Mean state gross moist stability (defined as the difference in moist static energy between 250hPa and 850hPa) in JJAS for the simulation with (a) CONTROL; (b) no bottom zonal asymmetries; (c) with land-sea contrast and topography; (d) east-west ocean heat fluxes only; (e) east-west ocean heat fluxes and land-sea contrast; (f) topography only; (g) east-west ocean heat fluxes and topography; (h) land-sea contrast only.

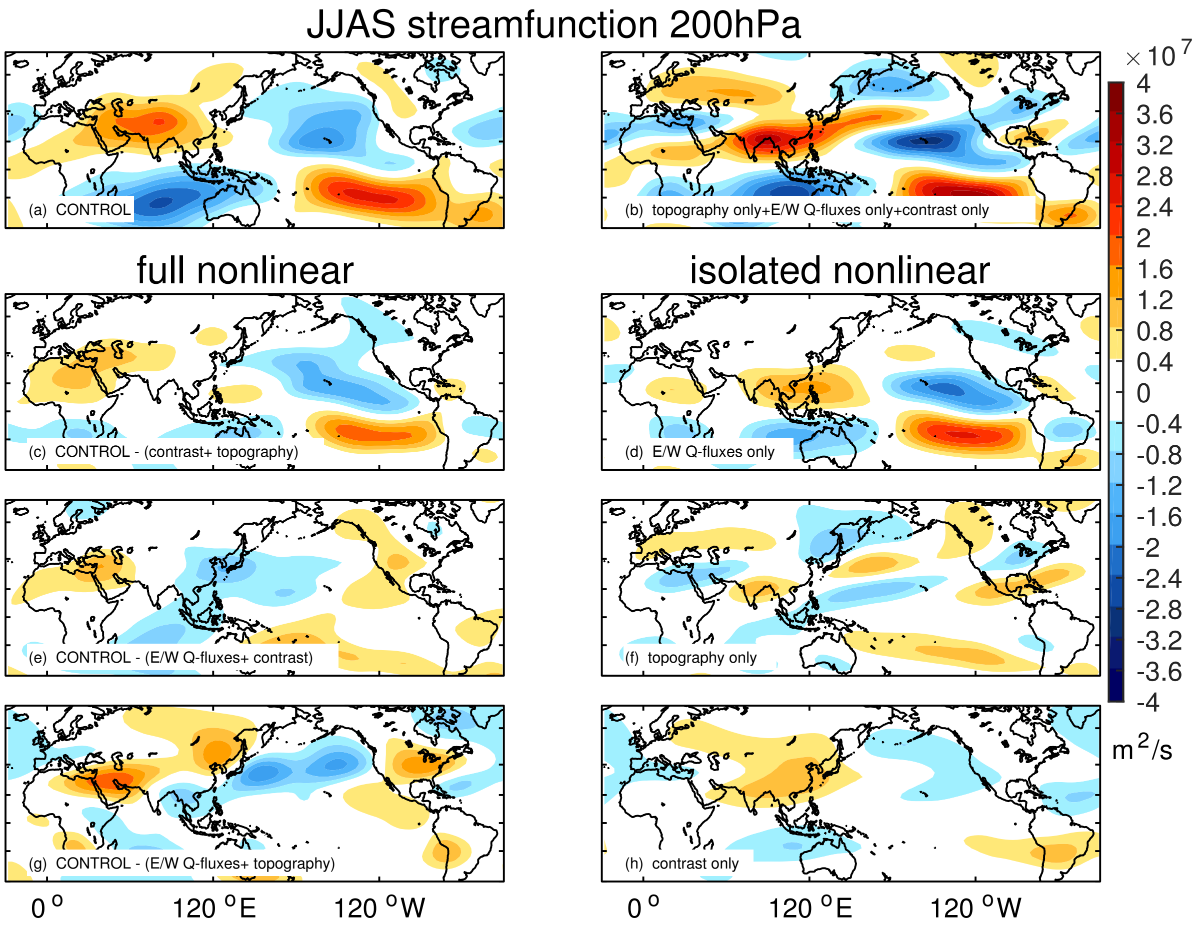

Figure 5. As in Figure 2 but for the deviation of June-September streamfunction at 200hPa from the zonal average.